

RESEARCH ARTICLE

More Precise Monitoring of Soil Moisture Content in Agricultural Fields by Upscaling Conversion of Multispectral Image Data From Unmanned Aerial Vehicles

YIFAN WANG¹, YI MA¹, FANGRONG ZHOU¹, ZUGUI HUANG^{1,2,3}, AND YIFEI YAO^{2,3}¹Electric Power Science Research Institute, Yunnan Power Grid Co., Ltd., Kunming 650217, China²Key Laboratory of Agricultural Soil and Water Engineering in Arid and Semiarid Areas, Ministry of Education, Northwest A&F University, Yangling, Shaanxi 712100, China³College of Water Resources and Architectural Engineering, Northwest A&F University, Yangling, Shaanxi 712100, China

Corresponding author: Yifei Yao (yifeiyao@nwsuaf.edu.cn)


This work was supported in part by the Science and Technology Project of China Southern Power Grid Yunnan Power Grid Co., Ltd. under Grant YNKJXM20220151, and in part by the Youth Fund of the National Natural Science Foundation of China under Grant 41804029.

ABSTRACT The utilization of unmanned aerial vehicle (UAV) remote sensing allows for fast and effective soil moisture content (SMC) monitoring. Scale conversion can obtain remote sensing images at multiple resolutions and offer the possibility of improving the estimation accuracy of SMC, which is crucial for precision agriculture. To explore the effect of upscaling conversion on SMC monitoring with UAV remote sensing, multispectral images and SMC data at different soil depths were acquired. The multispectral image with an original spatial resolution of 0.1 m was continuously upscaled to 6 m (with a step of 0.1 m and a total of 60 levels). The correlation coefficient method was adopted to determine the optimal scale, and spectral indices at the original and optimal scales were calculated. SMC inversion models at different depths were constructed at the original and optimal scales by multiple linear regression (MLR) and back propagation neural networks (BP), respectively. The results showed that the correlation of UAV multispectral data with SMC displayed a change in first enhancement and then fluctuating weakness with the increase of the upscaled levels. The optimal scale of UAV multispectral remote sensing for monitoring SMC at all soil depths was about 2 m. The BP models were significantly better than the MLR models. For example, in the SMC estimation at 0-20 cm, the RMSE of the BP model was reduced from 0.0110 to 0.0087 (20.9%). This study can provide theoretical and technical references for improving the accuracy of UAV multispectral remote sensing for SMC monitoring.

INDEX TERMS Unmanned aerial vehicle, soil moisture content, multispectral, upscaling conversion, multiple linear regression, back propagation neural network.

I. INTRODUCTION

The amount of water in the soil is expressed in terms of soil moisture content (SMC), which is divided into two types: gravimetric moisture content and volumetric moisture content. SMC is not only an important control of water,

The associate editor coordinating the review of this manuscript and approving it for publication was Turgay Celik .

carbon, and energy exchange between land and the atmosphere but also a major source of water absorption by crops and directly affects the recharge of surface and groundwater [1], [2], [3], [4], [5]. SMC monitoring in a rapid, accurate, and large area is significant for rational crop layout, crop growth and yield, precision irrigation, and the development of agricultural economies in arid and semi-arid areas [6], [7], [8], [9].

SMC can be divided into two types: mass moisture content and volumetric moisture content. Traditional SMC measurement methods, such as the heat pulse method [10], the drying method [11], and the time domain reflectometer (TDR) [12], allow for accurate measurements of soil samples. However, these methods can only work at the point scale and have obvious limitations in the measurement of large areas. In addition, most of these measurements are time-consuming and labor-intensive [13], damaging the original soil structure and making it difficult to ensure the synchronization of the measurement data.

SMC research based on remote sensing techniques has achieved the leap from point scale to surface scale and compensated for the deficiencies of traditional measurement methods. Since the emergence of remote sensing, SMC retrieval based on satellite remote sensing data has shown strong benefits and prospects at the regional scale and even globally [14], [15]. However, the relatively coarse resolution and long revisit times of satellite sensors limit their rapid and accurate acquisition of SMC at the farmland scale [16]. Fortunately, with the further development of remote sensing technology in recent years, the emergence of low-altitude unmanned aerial vehicles (UAVs) offers the possibility of overcoming the limitations of satellite remote sensing for SMC monitoring at the farmland scale. The UAV remote sensing technique for SMC monitoring has the advantages of being fast, non-destructive, and lower cost [17], [18], [19], [20]. Until now, many studies have demonstrated the effectiveness of SMC estimation with UAV remote sensing data [18], [21], [22], [23], [24]. However, in actual production activities, it is not usual to carry out multiple UAV flight operations to acquire remote sensing images at various spatial resolutions due to time and material cost constraints. This may result in the accuracy of soil moisture monitoring based on limited remote sensing image data being difficult to meet the application requirements. Therefore, a reasonable scale conversion of the acquired remote sensing product data at the original scale is necessary to meet various application needs, including but not limited to SMC monitoring.

Scale conversion in remote sensing is the process of transforming data or information from one scale to another; upscaling is the conversion from high resolution to low resolution, while downscaling is the reverse. Features typically exhibit different properties at different spatial geographic locations, and analyses based on remote sensing data also often need to consider spatial scale effects. Due to the differences in spatial heterogeneity at different scales, the estimation of SMC on the basis of remote sensing data has a large degree of uncertainty. Therefore, it is necessary to investigate the effect of scale on the estimation of SMC using remote sensing data to improve the accuracy of SMC detection and reduce operational costs in agricultural resource management. Furthermore, the relationship between SMC and vegetation or soil reflectance spectra frequently exhibits a non-linear regression due to the influence of factors such as vegetation cover, soil texture, and topography. Therefore,

the selection of appropriate regression algorithms is crucial to improving the estimation accuracy of SMC at different soil depths. Compared to traditional linear regression methods, artificial neural network models can capture the nonlinear relationships between different data sources and map the input-output relationships for any type of data. In this study, we combined a nonlinear back-propagation neural network algorithm on the basis of the upscaling of UAV multispectral remote sensing data in order to detect SMC information at different soil depths.

The aim of this study was to explore the effect of UAV multispectral data upscaled to different levels on SMC monitoring. For this purpose, we adopted the pixel aggregation method for continuous upscaling conversion of UAV multispectral images and acquired a total of 60 UAV multispectral images with different spatial resolutions, including the original resolution scale. The correlation coefficient method was used to determine the optimal scale, and spectral indices at the original and optimal scales were calculated. We analyzed the linear correlation of band reflectance and spectral indices at the original and optimal scale of UAV multispectral remote sensing data with SMC and screened out the band reflectance or spectral indices that were strongly correlated with SMC. Finally, we constructed SMC inversion models for different soil depths at the original and optimal scales by multiple linear regression and back-propagation neural networks, with the screened band reflectance or spectral index as the independent variable and SMC as the dependent variable, respectively. We hope to achieve rapid, high-precision, area-scale SMC monitoring to provide theoretical and technical support for managers to determine whether crops are suffering from water stress and adopt rational irrigation schemes to achieve water conservation and increase crop yields.

II. DATA AND METHODOLOGY

A. STUDY AREA

The study area was located at Jiefangzha of Hetao Irrigation Area in Inner Mongolia, China (Figure 1a), which has low rainfall and high evaporation all year round, and its soil type is mostly clay loam. The drainage capacity in the study area is weak due to the flat terrain. To efficiently utilize water resources and optimize the irrigation regime, it is necessary to monitor the SMC. Besides, during the test period, the feature type on the test site was mainly bare soil, and no crops had been planted yet, with only a few yellowed weeds after overwintering (Figure 1b).

B. SMC DATA

The collection of soil samples was conducted on 4/17/2019. Initially, we arranged 30 sampling points evenly on the experimental site (Figure 1b). Then, soil was collected vertically downward at 0-20 cm, 0-40 cm, and 0-60 cm depths with an auger. During the sampling process, the five-point sampling method was used to ensure the representativeness of the samples. Finally, we used the drying method (drying at a

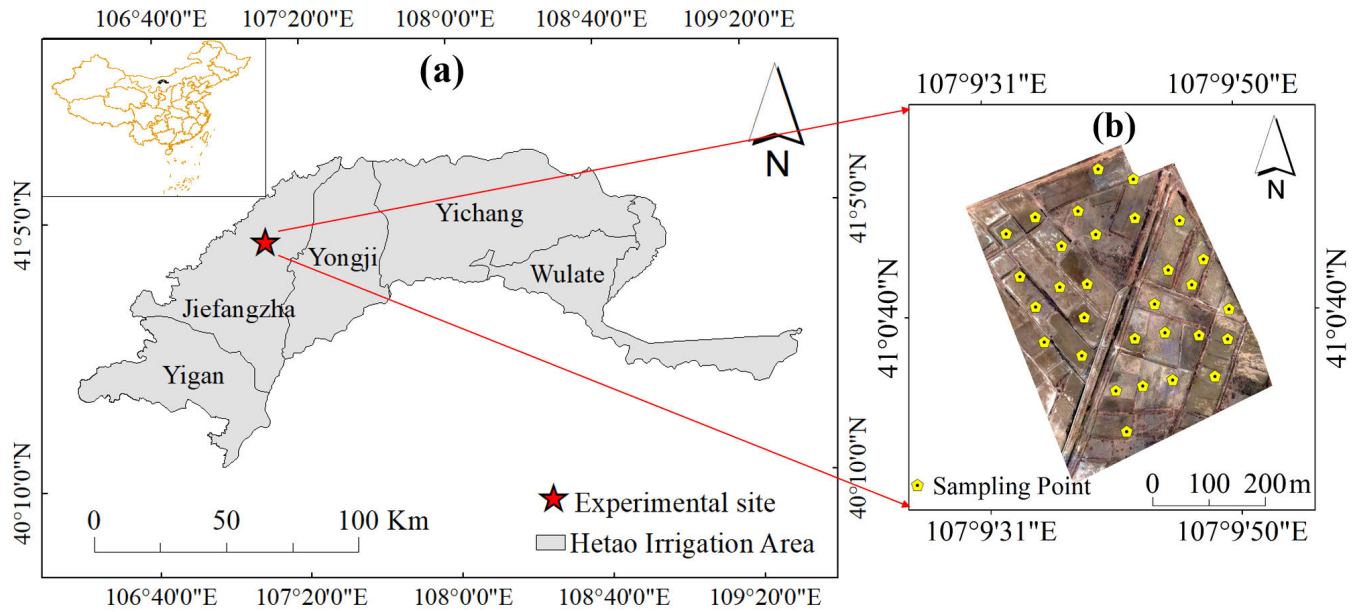


FIGURE 1. Study area location.

TABLE 1. The sensor parameters.

Weight (g)	Field of view (°)	Sensor size (mm)	Band	Name	Central wavelength (nm)	Spatial resolution (m)
530	38.26 × 30.97	6.66 × 5.32	1	Blue	490	0.1
			2	Green	550	
			3	Red	680	
			4	Red-edge	720	
			5	NIR1	800	
			6	NIR2	900	

constant temperature of 105 °C for 24 hours) to calculate the mass moisture content of the soil. The SMC is calculated by Equation (1).

$$SMC = (M_1 - M_2) / M_2 \times 100\% \quad (1)$$

where M_1 and M_2 represent the quality of wet and dry soil, respectively.

C. UAV MULTISPECTRAL IMAGE DATA

The M600 UAV from DJI Innovation Technology Ltd. was used to obtain multispectral remote sensing images. The UAV (including batteries) has a weight of 9.6 kg, maximum ascent and horizontal flight speeds of 5 and 18 m/s, respectively, and could withstand a maximum wind speed of 8 m/s with a maximum endurance of about 40 min. The sensor model is Micro-MCA, and some of the parameters are shown in Table 1. The operating time of the UAV was almost synchronized with the acquisition time of the soil samples. The flight altitude of the UAV was set to 120 m, and the spatial resolution of the acquired images was about 0.1 m. The acquired multispectral remote sensing images were stitched

and calibrated in the Pix4Dmapper software. After the radiometric calibration with a standard whiteboard, the reflectance of the sampling points was extracted.

D. SPECTRAL INDEX

In addition to the six bands provided by the UAV multispectral remote sensing images, some spectral indices for detecting soil information are introduced to improve the interpretation of SMC, and their formulas are shown in Table 2.

E. UPSCALING CONVERSION METHOD

The upscaling conversion method adopted in this study was pixel aggregation (PA). In the field of remote sensing, PA is an effective scale conversion method to compute based on an aggregation function and take the computed value as the pixel value of the converted low-resolution remote sensing image. Commonly used aggregation functions such as sum, maximum, minimum, and average are calculated as follows:

Let the sequence $x = \{x_1, \dots, x_m\}$, $x_i \in (-\infty, +\infty)$, $m \in \mathbb{N}^*$, $i = 1, 2, \dots, m$. The sum aggregation function can be

TABLE 2. Summary of spectral indices.

Spectral index	Calculation Formula	Reference
Salinity index 1 (SI1)	$\sqrt{G \times R}$	
Salinity index 2 (SI2-1)	$\sqrt{G^2 + R^2 + NIR1^2}$	[25]
Salinity index 3 (SI2-2)	$\sqrt{G^2 + R^2 + NIR2^2}$	
Salinity index (S2)	$\frac{(B - R)}{(B + R)}$	
Salinity index (S3)	$(G \times R) / B$	[26]
Salinity index (S4)	$\sqrt{B \times R}$	
Salinity index (S5)	$(B \times R) / G$	[27]
Normalized difference salinity index 1 (NDSI1)	$\frac{(R - NIR1)}{(R + NIR1)}$	[28]
Normalized difference salinity index 2 (NDSI2)	$\frac{(R - NIR2)}{(R + NIR2)}$	

Note: R = red, B = blue, and G = green.

expressed by Equation (2) as:

$$\text{Sum}(\mathbf{x}) = \sum_i^m x_i \quad (2)$$

The maximum aggregation function can be expressed by Equation (3) as:

$$\text{Max}(\mathbf{x}) = \max \{x_1, x_2, \dots, x_m\} \quad (3)$$

Similarly, the minimum aggregation function can be expressed by Equation (4) as:

$$\text{Min}(\mathbf{x}) = \min \{x_1, x_2, \dots, x_m\} \quad (4)$$

In this study, mean aggregation was adopted for the upscaling conversion of UAV multispectral remote sensing data, which can maintain the image information relatively well. The mean aggregation function is represented by Equation (5) as:

$$M(\mathbf{x}) = \frac{1}{m} \sum_{i=1}^m x_i \quad (5)$$

The two-dimensional form of Equation (5) can be further expressed by Equation (6) as:

$$M'(\mathbf{x}) = \frac{1}{mn} \sum_{i=1}^m \left(\sum_{j=1}^n x_{ij} \right) \text{ with } \mathbf{x} = \begin{pmatrix} x_{11} & \dots & x_{1n} \\ \vdots & \ddots & \vdots \\ x_{m1} & \dots & x_{mn} \end{pmatrix} \quad (6)$$

For the digital images of remote sensing, the single band is represented as a two-dimensional matrix, and then the band

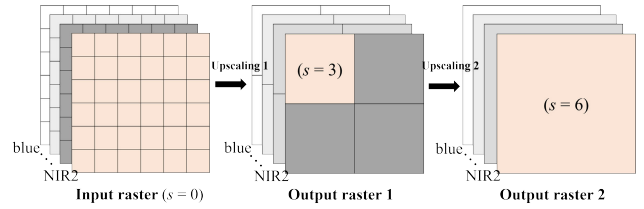


FIGURE 2. The upscaling conversion of a high-resolution image to a low-resolution image (note that $n = m, n \in \mathbf{N}^*$, and when the pixel coefficient value is set to s , it makes the size of the output pixel s times larger than the original input pixel).

reflectance that is upscaled to the s^{th} level can be calculated by Equation (7) as:

$$b_{u,s} = M'(\mathbf{b}) \text{ with } \mathbf{b} = \begin{pmatrix} b_{11} & \dots & b_{1n} \\ \vdots & \ddots & \vdots \\ b_{m1} & \dots & b_{mn} \end{pmatrix} \quad (7)$$

where $b_{u,s}$ is the u -band of the UAV multispectral image that is upscaled to the s^{th} level, and u is blue, green, red, red-edge, NIR1, and NIR2 in this study; \mathbf{b} is the pixel value within the $n \times m$ window of the high-resolution UAV multispectral remote sensing image, and $b_{ij} \in [-1, 1]$.

The upscaling conversion of the UAV multispectral remote sensing image is shown in Figure 2, and this work was conducted using the ‘‘arcpy’’ package in Python 2.7.

F. MODELING AND ASSESSMENT

1) MULTIPLE LINEAR REGRESSION (MLR)

MLR analysis is one of the most commonly used statistical methods for measuring the relationship between multiple variables and predicting the behavior of the dependent variable based on multiple independent variables [29]. In general, the MLR model is given by Equation (8).

$$Y = \beta_0 + \beta_k X_k \quad (8)$$

where Y is the dependent variable, which in this study is SMC at different depths; β_0 is the regression constant; β_k is the overall regression parameter; and X_k is the independent variable, which in this study is the band reflectance or the spectral index.

2) BACK PROPAGATION NEURAL NETWORK (BP)

BP is a neural network that is trained based on error back propagation [30]. The BP model generally consists of an input layer, a hidden layer, and an output layer. Besides, the model has a relatively strong ability for self-learning and nonlinear mapping [31], is widely used in various fields, and has better performance in soil moisture content estimation. The BP model is constructed as follows:

Let there be n training samples, each with m indicators. Then the initial information matrix is:

$$A' = (a'_{ij})_{n \times m} \quad (9)$$

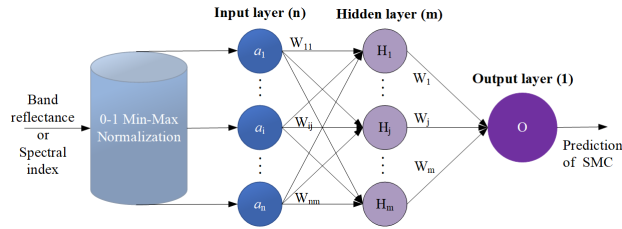


FIGURE 3. Topology of SMC inversion model based on BP neural network algorithm.

where $i = 1, 2, \dots, n; j = 1, 2, \dots, m; x_{ij}$ represents the value of the j^{th} indicator of the i^{th} training sample.

The first step is to eliminate the dimension between different indicators (band reflectance, spectral index, and SMC) by Equation (10)

$$a_{ij} = \frac{a'_{ij} - \min_{i=1}^n a'_{ij}}{\max_{i=1}^n a'_{ij} - \min_{i=1}^n a'_{ij}} \quad (10)$$

Then we can obtain the dimensionless matrix $A = (a_{ij})_{n \times m}$. The next step is to determine the calculations of the hidden and output layers. The hidden layer is calculated by Equation (11)

$$H_j = f\left(\sum_{i=1}^m a_i \cdot W_{ij}\right) \quad (11)$$

The transfer function of the hidden layer in Equation (11) is calculated by Equation (12)

$$f(x) = \frac{1}{1 + e^{-\alpha x}} \quad (12)$$

where $\alpha = 1$.

The output layer is calculated by Equation (13)

$$O = f\left(\sum_{j=1}^m H_j \cdot W_j\right) \quad (13)$$

The transfer function of the output layer in Equation (13) is linear, which is calculated by Equation (14)

$$f(x) = x \quad (14)$$

The topology of the BP-based SMC inversion model in this study is shown in Figure 3.

3) INDICATORS FOR MODEL EVALUATION

The correlation of band reflectance and spectral index with SMC is measured by Pearson’s correlation coefficient (r). The absolute value of Pearson’s correlation coefficient is adopted to determine the optimal scale for SMC monitoring by UAV multispectral remote sensing and the input variables for the SMC inversion model. The R^2 and RMSE are used to evaluate the accuracy of the model. The closer R^2 is to 1 and the closer RMSE is to 0, the more accurate the model is. R^2 ,

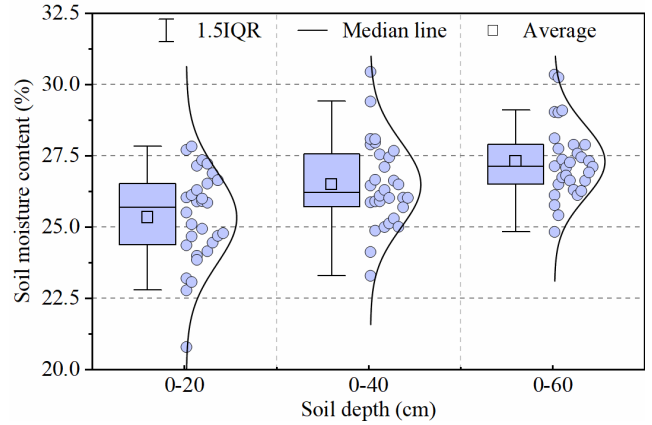


FIGURE 4. Statistical characteristics of SMC.

RMSE, and r can be calculated from Equations (15), (16), and (17), respectively.

$$R^2 = \frac{\sum_{i=1}^n (\hat{S}_i - \bar{S})^2}{\sum_{i=1}^n (S_i - \bar{S})^2} \quad (15)$$

$$RMSE = \sqrt{\frac{\sum_{i=1}^n (\hat{S}_i - S_i)^2}{n}} \quad (16)$$

$$r = \frac{\sum_{i=1}^n (S_i - \bar{S})(S' - \bar{S}')}{\left[\sum_{i=1}^n (S_i - \bar{S})^2 \sum_{i=1}^n (S' - \bar{S}')^2\right]^{1/2}} \quad (17)$$

where \hat{S}_i represents the estimated SMC value, S_i represents the measured SMC value, \bar{S} represents the average value of SMC, S' represents the band reflectance or spectral index, and \bar{S}' represents the average value of the band reflectance or spectral index.

III. RESULTS

A. STATISTICAL CHARACTERIZATION OF SMC

As can be seen in Figure 4, the SMC of the experimental site at the depth of 0-20 cm was in the range of 20%-28% overall; that was in the range of 23%-31% at 0-40 cm; and that was approximately in the range of 25%-31% at 0-60 cm. In other words, the moisture in the soil increased as the depth of the soil increased. The statistical characteristics of SMC are shown in Figure 4.

B. DETERMINATION OF THE OPTIMAL UPSCALED LEVEL

First, the 6-band reflectance of the UAV multispectral data with a spatial resolution of $0.1 \text{ m} \times 0.1 \text{ m}$ (original scale, denoted as the 1st level) was upscaled to $6 \text{ m} \times 6 \text{ m}$ (denoted as the 60th level) with a step of 0.1 m. Second, the bands upscaled to different levels were analyzed for Pearson’s correlation with the SMC at different depths, respectively. Last, the optimal upscaled level was determined as the level

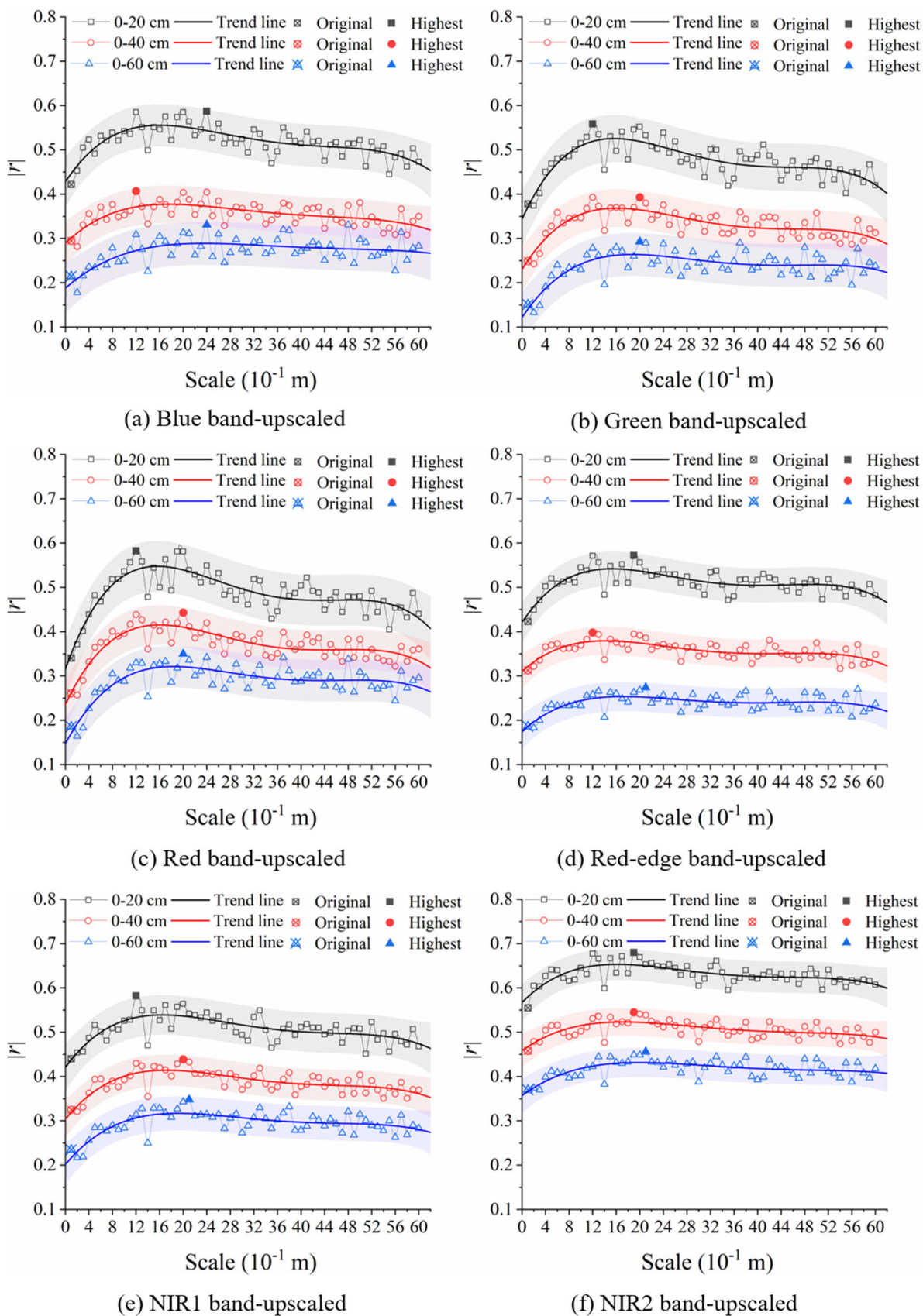


FIGURE 5. Correlation of UAV band reflectance that upscaled conversion to different levels with SMC at different soil depths ($|r|$ is the absolute value of Pearson's correlation coefficient, the same as below).

TABLE 3. Correlations of band reflectance with SMC at different soil depths for original and optimal upscaled UAV multispectral data.

Soil depth (cm)	Type	Upscaled band reflectance					
		Blue	Green	Red	Red-edge	NIR1	NIR2
	Original scale (m)	0.1	0.1	0.1	0.1	0.1	0.1
0-20	Original correlation	0.422*	0.378*	0.340	0.423*	0.440*	0.555**
	Optimal scale (m)	1.9	1.9	1.9	1.9	1.9	1.9
	Optimal correlation	0.522**	0.546**	0.581**	0.572**	0.557**	0.680**
0-40	Original correlation	0.295	0.249	0.261	0.313	0.325	0.458*
	Optimal scale (m)	1.9	1.9	1.9	1.9	1.9	1.9
	Optimal correlation	0.355*	0.370*	0.420*	0.395*	0.429*	0.545**
0-60	Original correlation	0.215	0.151	0.186	0.186	0.235	0.370*
	Optimal scale (m)	2.1	2.1	2.1	2.1	2.1	2.1
	Optimal correlation	0.311	0.290	0.336	0.274	0.348	0.456*

Note. * $p < 0.05$, ** $p < 0.01$, and *** $p < 0.001$, the same below.

corresponding to the band reflectance that had the highest correlation with the SMC during the upscaling.

The $|r|$ between band reflectance and SMC showed a tendency to first increase and then fluctuate downward as the upscaled level increased. Among the six upscaled bands correlating with the SMC, NIR2 demonstrated the most pronounced correlation in all depths (Figure 5f). Therefore, the level corresponding to the highest $|r|$ between the NIR2 and SMC during the upscaling was taken as the optimal upscaled level for each band. The $|r|$ of the NIR2 band with the SMC at 0-20 cm and 0-40 cm reached its highest (0.680 and 0.545) at the upscaling to the 19th level (i.e., 1.9 m), and its $|r|$ with the SMC at 0-60 cm depths was highest (0.456) at the 21st level (i.e., 2.1 m). Therefore, 1.9 m was the optimal scale of UAV multispectral data for monitoring SMC at 0-20 cm and 0-40 cm soil depths, while 2.1 m was the optimal scale for monitoring SMC at 0-60 cm. The correlations of the band reflectance at the original and optimal scales with the SMC at different depths are shown in Table 3.

C. CORRELATION ANALYSIS OF SPECTRAL INDEX WITH SMC

The spectral indices calculated based on band reflectance at the original and optimal scales were subjected to Pearson correlation analysis with the SMC, respectively, and the results are shown in Figure 6.

Compared with the spectral indices at the original scale, those at the optimal scale (except NDSI1) exhibited stronger correlations with the SMC at different depths. In other words, the upscaling conversion can improve the correlation of UAV multispectral data with SMC. For example, among the correlations of these indices with the SMC at 0-20 cm depth (Figure 6a and b), SI1, SI2-1, SI2-2, S3, S4, and S5 showed the most significant enhancement, with correlation coefficients strengthening from around -0.4 to

-0.6 . However, S3 and NDSI2 displayed only a very small increase, and NDSI1 showed a relatively significant decrease. In addition, the correlations between spectral indices and SMC gradually weakened as the depth increased, showing 0-20 cm > 0-40 cm > 0-60 cm.

D. SELECTION OF INPUT VARIABLES FOR THE SMC INVERSION MODEL

The $|r|$ of the band reflectance and spectral index with SMC at the original scale were ranked in descending order, and the band or spectral index in the last one-third of the sequence would be used as the input variables for the model.

As can be seen from Figure 7, the optimal combinations of input variables for the SMC inversion model at 0-20 cm, 0-40 cm, and 0-60 cm for the original scale were, respectively, SI2-2, Blue, Red-edge, NIR1, and NIR2; Blue, S5, Red-edge, NIR1, and NIR2; and Blue, NIR1, NDSI2, S5, and NIR2. Obviously, the bands or spectral indices that were sensitive to the SMC at different depths were in general agreement. The input variables of the model at the optimal scale remain consistent with the original scale.

E. SMC INVERSION MODELS BASE ON MLR

Multiple linear regression was employed to construct SMC inversion models at the original and optimal scale with SMC at different soil depths as the dependent variable, and the results are presented in Figure 8.

The estimation accuracy of SMC based on UAV multispectral data at the optimal scale significantly outperformed that using UAV multispectral data at the original scale. For example, in the estimation of SMC at 0-20 cm, the R^2 of the MLR model improved most significantly from 0.437 at the original scale to 0.573 at the optimal scale. Besides, the R^2 of the MLR models at 0-40 cm and 0-60 cm also showed a relatively significant enhancement.

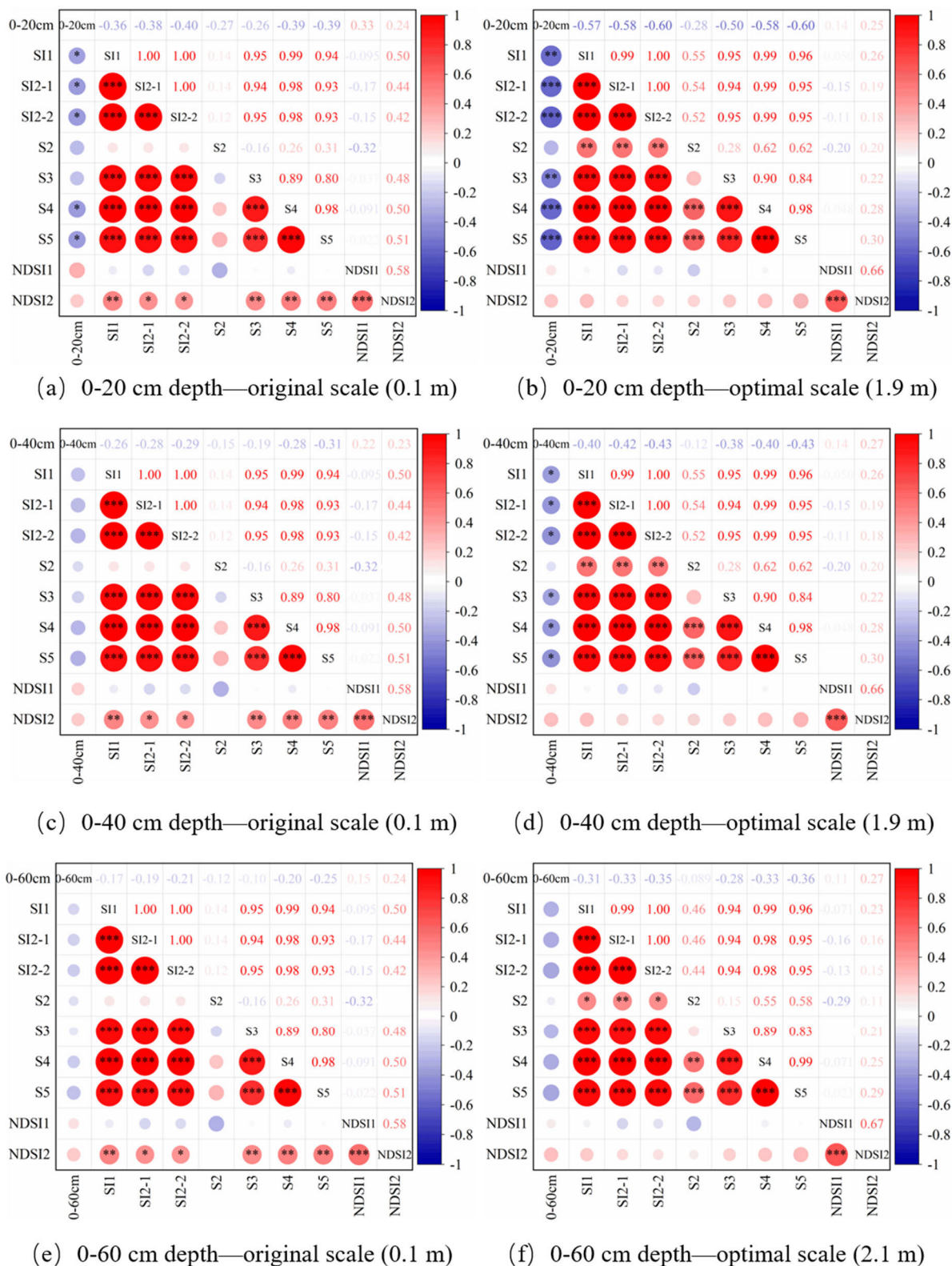


FIGURE 6. Correlation matrix of spectral indices with SMC at different soil depths for original and optimal upscaled UAV multispectral data.

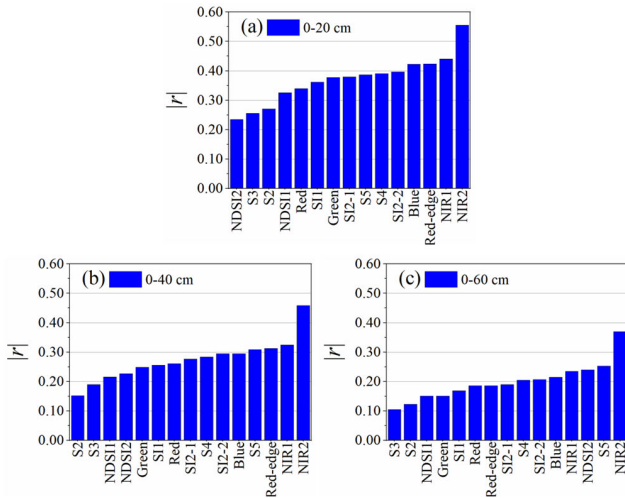


FIGURE 7. Correlation matrix of spectral indices with SMC at different soil depths for original and optimal upscaled UAV multispectral data.

TABLE 4. The expressions of MLR models at different depths.

Soil depth (cm)	MLR model	
	Original scale	Optimal scale
0-20	$Y = 0.316 + 0.065 \times (SI2-2) - 0.263 \times Blue + 0.074 \times (Red-edge) + 0.123 \times NIR1 - 0.423 \times NIR2$	$Y = 0.315 + 0.069 \times (SI2-2) - 0.257 \times Blue - 0.009 \times (Red-edge) + 0.266 \times NIR1 - 0.463 \times NIR2$
0-40	$Y = 0.321 - 0.075 \times Blue - 0.038 \times S5 + 0.102 \times (Red-edge) + 0.133 \times NIR1 - 0.399 \times NIR2$	$Y = 0.323 + 0.228 \times Blue - 0.241 \times S5 + 0.068 \times (Red-edge) + 0.101 \times NIR1 - 0.348 \times NIR2$
0-60	$Y = 0.269 + 0.165 \times Blue - 0.313 \times S5 + 0.131 \times NDSI2 + 0.043 \times NIR1 + 0.029 \times NIR2$	$Y = 0.264 + 0.412 \times Blue - 0.499 \times S5 + 0.157 \times NDSI2 + 0.062 \times NIR1 - 0.002 \times NIR2$

In the SMC estimations at 0-20 cm, 0-40 cm, and 0-60 cm, the RMSE of the MLR models were 0.0120, 0.0121, and 0.0105 at the original scale, and 0.0105, 0.0113, and 0.0097 at the optimal scale, with a decrease of 12.5%, 6.61%, and 7.62%, respectively. Besides, the estimation accuracy of SMC, whether based on the UAV multispectral data at the original or optimal upscaled levels, showed a gradual decrease as the depth increased, exhibiting 0-20 cm > 0-40 cm > 0-60 cm. The expressions of the MLR models at different soil depths are shown in Table 4.

F. SMC INVERSION MODELS BASE ON BP

The BP neural network was adopted to construct the SMC inversion model at the original and optimal scale, and the results are shown in Figure 9. The R² of the BP models increased from 0.526, 0.439, and 0.402 at the original scale to 0.706, 0.539, and 0.439 at the optimal scale for the three soil depths, respectively. The RMSE was reduced from 0.0110, 0.0111, and 0.0098 at the original scale to 0.0087, 0.0101, and

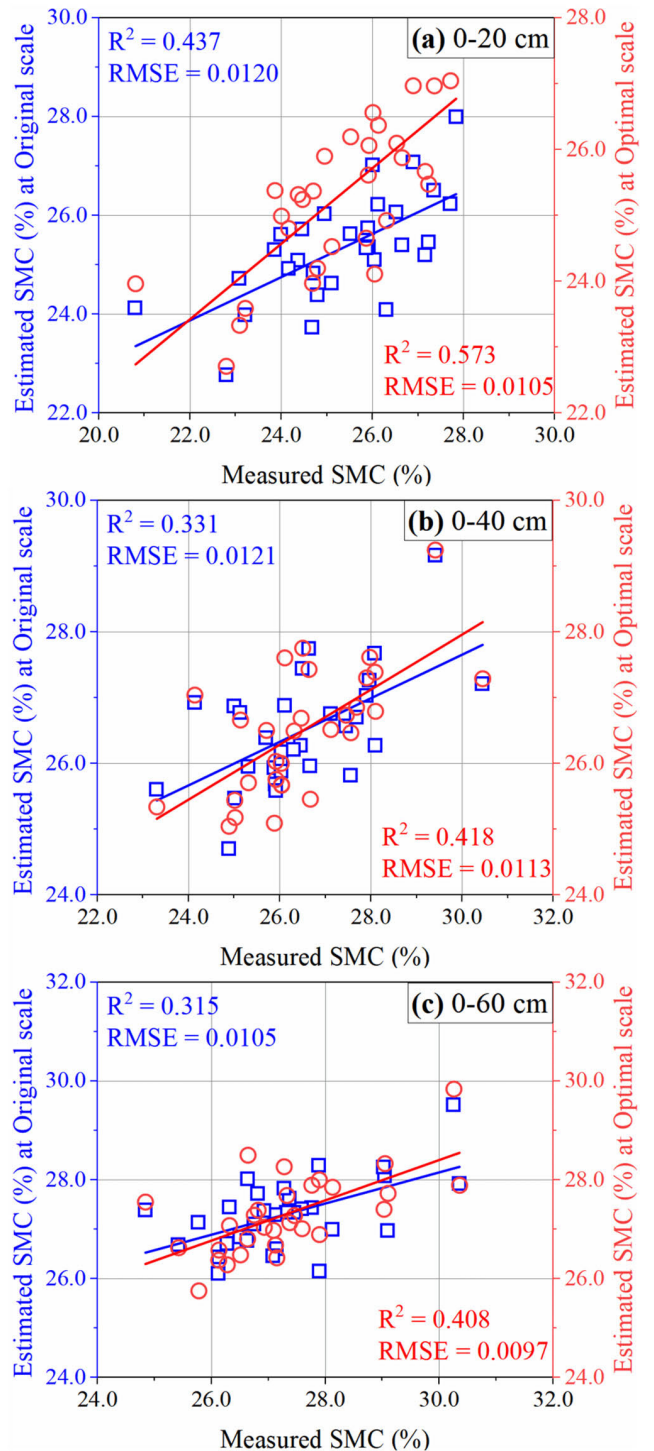


FIGURE 8. MLR models at different soil depths constructed using the original and optimal upscaled UAV multispectral data.

0.0089 at the optimal scale, with a reduction of 20.9%, 9.0%, and 9.2%, respectively. The nonlinear BP model significantly outperformed the multiple linear regression model.

G. PREDICTED SOIL MOISTURE CONTENT MAP

Compared with the complex non-linear BP neural network model, the multiple linear regression model is simple and

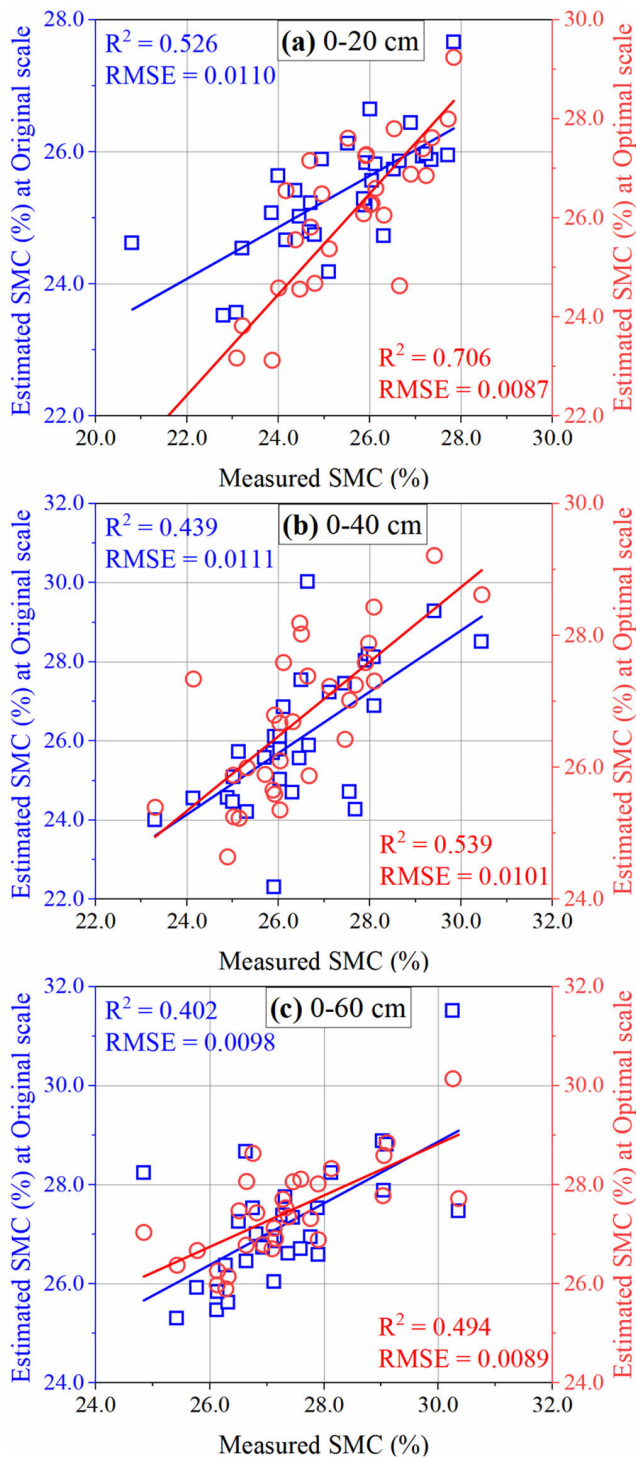


FIGURE 9. BP models at different depths constructed using the original and optimal upscaled UAV multispectral data.

provides specific model expressions (Table 4). Therefore, in this study, the SMC distribution map at different soil depths in the study area was predicted based on multiple linear regression models developed at the original and optimal scales, respectively.

As can be seen from Figure 10, compared with the SMC predicted using the multispectral image data at the original scale, those predicted with the multispectral image data at the optimal scale were closer to the measured SMC values. Therefore, it is of great significance to improve the performance of UAV sensors for monitoring SMC by upscaling the conversion of the original image data.

IV. DISCUSSION

SMC estimation based on optical remote sensing data is affected by a variety of factors, such as weather conditions, cloud cover, vegetation cover, soil roughness, and topography [32], [33], [34], [35]. Compared with satellite remote sensing, UAVs are flexible and controllable, and their lower flight altitude can greatly reduce the influence of cloud cover during work, which gives them a significant advantage in SMC estimation at the field scale. However, generally, during the UAV work, multiple flight altitudes are not set to acquire a large number of remote sensing images because multiple operations would increase the cost a lot. To break through this limitation, we performed a continuous-scale conversion of the original UAV multispectral data. The optimal scales for SMC monitoring at different depths were also determined while acquiring multiple remote sensing images, and the estimation accuracy of SMC was significantly improved. In this study, both the BP model and the MLR model showed considerable estimation accuracy. It is worth mentioning that we assumed the independence of the variables (band reflectance and spectral index) in the construction of the MLR model. However, in fact, there may be a linear correlation between them. The MLR model between the dependent variable Y and the independent variables X_1 and X_2 may also be $Y = \beta_0 + \beta_1 X_1 + \beta_2 X_2 + \beta_3 X_1 \cdot X_2$. More forms of regression should be considered in the future to improve the accuracy of regression analyses.

The main upscaling methods for remote sensing images are the nearest neighbor method, the empirical regression method, the Bayesian method, and the physical modeling method. The nearest neighbor method takes the average of the neighboring four pixels of the original pixel as the upscaled converted pixel, which loses a large amount of pixel information despite having significant computational efficiency. The Bayesian method is an upscaling method based on the maximum entropy method, which requires the incorporation of certain prior knowledge and makes it more difficult to implement. The portability of the empirical regression method is relatively poor because it relies on a large number of historical observations. Theoretically, the physical modeling method works best, but such physical model-based scale conversions are typically difficult to construct due to model assumptions and parameter uncertainties. In this study, we adopted mean-aggregation for the upscaling of UAV multispectral images. The advantage of this approach is that all input pixel information at each given scale is considered during the upscaling, and the soil reflectance information associated with SMC can be better preserved without additional artificial weighting.

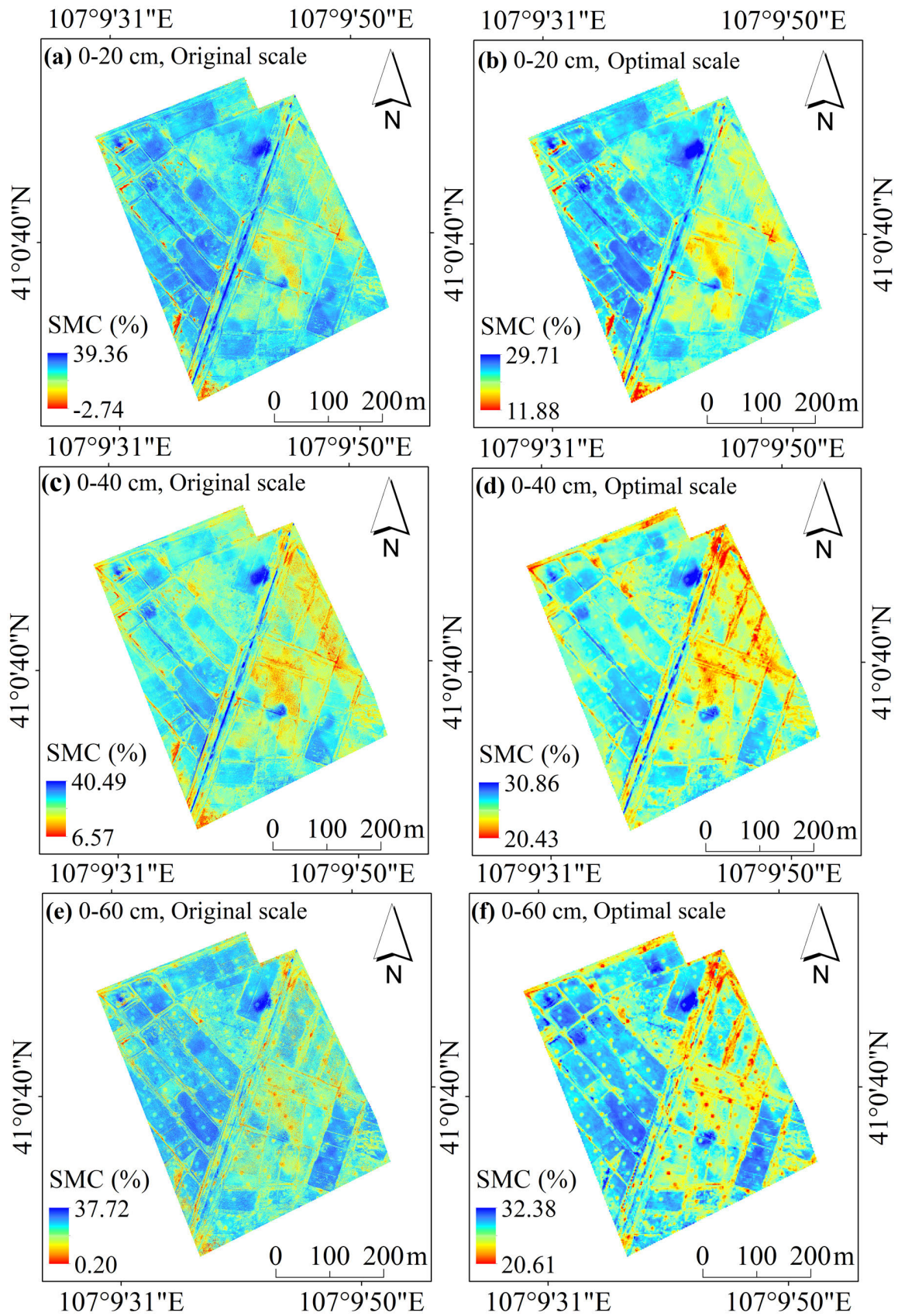


FIGURE 10. SMC prediction maps for the study area based on multiple linear regression models at the original and optimal scales.

Among the 60 upscaled levels, the correlation between the band reflectance of UAV multispectral data and SMC varied at different scales, and the essence of this result is the difference in field heterogeneity. In SMC monitoring based on remote sensing methods, higher spatial heterogeneity typically leads to lower estimation accuracy. It was interesting to note that the $|r|$ between band reflectance and SMC showed a tendency to first increase and then fluctuate downward as the upscaled level increased. This variation in correlation was largely because the field heterogeneity corresponding to the scale exhibited an initial decline and then a fluctuating increase. It can be predicted that the correlation between remote sensing data and SMC would not be the strongest at either infinitely small or large scales of monitoring. Additionally, when the scale is further inflated, the correlation of UAV multispectral data with SMC still tends to undulatingly decrease but does not approach 0. Because more feature elements are incorporated (e.g., vegetation, rocks, etc.), the heterogeneity fluctuates and increases further. The NIR2 band reflectance, which has the highest correlation with SMC, was taken as the standard for the determination of the optimal upscaled level during the upscaling of the UAV multispectral data. The optimal scale of UAV multispectral data for SMC monitoring at various depths in agricultural areas with no vegetation cover is about 2 m. For the other bands (e.g., green, red, red-edge, and NIR1), although the upscaled levels corresponding to the highest correlations with SMC at different depths were not exactly the same, these levels were generally around the 20th level. In other words, there is similarity in the optimal upscaled levels for each band, which is likely to facilitate the rapid determination of the optimal scale for other bands. Further research work in this area could be carried out in the future.

Compared with performing multiple UAV works to obtain a suitable resolution scale for detecting SMC, this study achieved better performance in SMC monitoring by only applying an upscaling conversion to limited UAV multispectral data. In other words, our study can provide theoretical and technical support for reducing measurement costs in agricultural resource management. However, it is worth mentioning that this study did not consider the effects of factors such as vegetation, topography, and soil roughness, which may make it problematic to generalize the proposed model to other regions with more complex land characteristics, and further research could be carried out in this direction in the future.

V. CONCLUSION

This study aimed to investigate the effect of the upscaling conversion of UAV multispectral data on SMC monitoring at different soil depths. The results demonstrated that the upscaling conversion of UAV multispectral data can significantly improve the estimation accuracy of SMC. The correlation of UAV multispectral data with SMC displayed a change in first enhancement and then fluctuating weakness with the increase of the upscaled levels. Apparently, compared with SMC estimation using UAV multispectral data

at the original scale, there was a more optimal scale that could significantly improve the estimation accuracy of SMC at different soil depths. In this study, this scale was about 2 m. This study can provide theoretical and technical support for improving the estimation accuracy of SMC in agricultural fields based on UAV multispectral remote sensing and reducing measurement costs in agricultural resource management.

REFERENCES

- [1] Y. Zhang, S. Liang, Z. Zhu, H. Ma, and T. He, "Soil moisture content retrieval from Landsat 8 data using ensemble learning," *ISPRS J. Photogramm. Remote Sens.*, vol. 185, pp. 32–47, Mar. 2022.
- [2] J. Liang, G. Liang, Y. Zhao, and Y. Zhang, "A synergic method of Sentinel-1 and Sentinel-2 images for retrieving soil moisture content in agricultural regions," *Comput. Electron. Agricult.*, vol. 190, Nov. 2021, Art. no. 106485.
- [3] E. Babaeian, M. Sadeghi, S. B. Jones, C. Montzka, H. Vereecken, and M. Tuller, "Ground, proximal, and satellite remote sensing of soil moisture," *Rev. Geophys.*, vol. 57, no. 2, pp. 530–616, Jun. 2019.
- [4] P. Viterbo and A. K. Betts, "Impact of the ECMWF reanalysis soil water on forecasts of the July 1993 Mississippi flood," *J. Geophys. Res., Atmos.*, vol. 104, no. 16, pp. 19361–19366, Aug. 1999.
- [5] Y. Kim, H. Park, J. S. Kimball, A. Colliander, and M. F. McCabe, "Global estimates of daily evapotranspiration using SMAP surface and root-zone soil moisture," *Remote Sens. Environ.*, vol. 298, Dec. 2023, Art. no. 113803.
- [6] G. O. Awe, J. M. Reichert, L. C. Timm, and O. O. Wendroth, "Temporal processes of soil water status in a sugarcane field under residue management," *Plant Soil*, vol. 387, nos. 1–2, pp. 395–411, Feb. 2015.
- [7] J. Guo, Q. Bai, W. Guo, Z. Bu, and W. Zhang, "Soil moisture content estimation in winter wheat planting area for multi-source sensing data using CNNR," *Comput. Electron. Agricult.*, vol. 193, Feb. 2022, Art. no. 106670.
- [8] M. El Hajji, N. Baghdadi, M. Zribi, and H. Bazzi, "Synergic use of Sentinel-1 and Sentinel-2 images for operational soil moisture mapping at high spatial resolution over agricultural areas," *Remote Sens.*, vol. 9, no. 12, p. 1292, Dec. 2017.
- [9] N. Mahmoudi, A. Majidi, M. Jamei, M. Jalali, S. Maroufpoor, J. Shiri, and Z. M. Yaseen, "Mutating fuzzy logic model with various rigorous meta-heuristic algorithms for soil moisture content estimation," *Agricult. Water Manag.*, vol. 261, Mar. 2022, Art. no. 107342.
- [10] N. S. Rakesh, A. Ahmed, J. Joseph, R. S. Aouti, M. Mogra, A. Kushwaha, R. Ashwin, S. M. Rao, and G. K. Ananthasuresh, "Analysis of heat paths in dual-probe-heat-pulse soil-moisture sensors for improved performance," *Sens. Actuators A, Phys.*, vol. 318, Feb. 2021, Art. no. 112520.
- [11] B. C. O'Kelly and V. Sivakumar, "Water content determinations for peat and other organic soils using the oven-drying method," *Drying Technol.*, vol. 32, no. 6, pp. 631–643, Apr. 2014.
- [12] M. Bittelli, F. Tomei, P. Anbazhagan, R. R. Pallapati, P. Mahajan, C. Meisina, M. Bordoni, and R. Valentino, "Measurement of soil bulk density and water content with time domain reflectometry: Algorithm implementation and method analysis," *J. Hydrol.*, vol. 598, Jul. 2021, Art. no. 126389.
- [13] R. Gangat, H. Van Deventer, L. Naidoo, and E. Adam, "Estimating soil moisture using Sentinel-1 and Sentinel-2 sensors for dryland and palustrine wetland areas," *South Afr. J. Sci.*, vol. 116, no. 7, p. 9, Jul. 2020.
- [14] H. Adab, R. Morbidelli, C. Saltalippi, M. Moradian, and G. A. F. Ghalhari, "Machine learning to estimate surface soil moisture from remote sensing data," *Water*, vol. 12, no. 11, p. 3223, Nov. 2020.
- [15] L. Luo, Y. Li, F. Guo, Z. Huang, S. Wang, Q. Zhang, Z. Zhang, and Y. Yao, "Research on robust inversion model of soil moisture content based on GF-1 satellite remote sensing," *Comput. Electron. Agricult.*, vol. 213, Oct. 2023, Art. no. 108272.
- [16] X. Zhao, J. Zhong, J. Hu, L. Wu, and X. Chen, "Bismuth terephthalate induced Bi(0) for enhanced RhB photodegradation and 4-nitrophenol reduction," *J. Phys. Chem. Solids*, vol. 111, pp. 431–438, Dec. 2017.
- [17] S. Zhu, N. Cui, H. Jin, X. Jin, L. Guo, S. Jiang, Z. Wu, M. Lv, F. Chen, Q. Liu, and M. Wang, "Optimization of multi-dimensional indices for kiwifruit orchard soil moisture content estimation using UAV and ground multi-sensors," *Agricult. Water Manag.*, vol. 294, Apr. 2024, Art. no. 108705.

- [18] Y. Gao, X. Lian, and L. Ge, "Inversion model of surface bare soil temperature and water content based on UAV thermal infrared remote sensing," *Infr. Phys. Technol.*, vol. 125, Sep. 2022, Art. no. 104289.
- [19] E. Babaeian, S. Paheding, N. Siddique, V. K. Devabhaktuni, and M. Tuller, "Estimation of root zone soil moisture from ground and remotely sensed soil information with multisensor data fusion and automated machine learning," *Remote Sens. Environ.*, vol. 260, Jul. 2021, Art. no. 112434.
- [20] O. Wigmore, B. Mark, J. McKenzie, M. Baraer, and L. Lutz, "Sub-metre mapping of surface soil moisture in proglacial valleys of the tropical Andes using a multispectral unmanned aerial vehicle," *Remote Sens. Environ.*, vol. 222, pp. 104–118, Mar. 2019.
- [21] L. Hassan-Esfahani, A. Torres-Rua, A. Jensen, and M. McKee, "Assessment of surface soil moisture using high-resolution multi-spectral imagery and artificial neural networks," *Remote Sens.*, vol. 7, no. 3, pp. 2627–2646, Mar. 2015.
- [22] X. Ge, J. Wang, J. Ding, X. Cao, Z. Zhang, J. Liu, and X. Li, "Combining UAV-based hyperspectral imagery and machine learning algorithms for soil moisture content monitoring," *PeerJ*, vol. 7, p. e6926, May 2019.
- [23] M. Cheng, X. Jiao, Y. Liu, M. Shao, X. Yu, Y. Bai, Z. Wang, S. Wang, N. Tuohuti, S. Liu, L. Shi, D. Yin, X. Huang, C. Nie, and X. Jin, "Estimation of soil moisture content under high maize canopy coverage from UAV multimodal data and machine learning," *Agricult. Water Manag.*, vol. 264, Apr. 2022, Art. no. 107530.
- [24] F. Lu, Y. Sun, and F. Hou, "Using UAV visible images to estimate the soil moisture of steppe," *Water*, vol. 12, no. 9, p. 2334, Aug. 2020.
- [25] J. A. A. Abbas, "Soil salinity assessment by using spectral salinity indices in al-sweira project middle of the Iraqi alluvial plain," *Int. J. Environ. Sci. Technol.*, vol. 20, no. 10, pp. 10847–10860, Oct. 2023.
- [26] A. Abbas, S. Khan, N. Hussain, M. A. Hanjra, and S. Akbar, "Characterizing soil salinity in irrigated agriculture using a remote sensing approach," *Phys. Chem. Earth, Parts A/B/C*, vols. 55–57, pp. 43–52, Jan. 2013.
- [27] A. Allbed, L. Kumar, and Y. Y. Aldakheel, "Assessing soil salinity using soil salinity and vegetation indices derived from IKONOS high-spatial resolution imageries: Applications in a date palm dominated region," *Geoderma*, vols. 230–231, pp. 1–8, Oct. 2014.
- [28] N. Yang, S. Yang, W. Cui, Z. Zhang, J. Zhang, J. Chen, Y. Ma, C. Lao, Z. Song, and Y. Chen, "Effect of spring irrigation on soil salinity monitoring with UAV-borne multispectral sensor," *Int. J. Remote Sens.*, vol. 42, no. 23, pp. 8952–8978, Dec. 2021.
- [29] Y. Lee, C. Jung, and S. Kim, "Spatial distribution of soil moisture estimates using a multiple linear regression model and Korean geostationary satellite (COMS) data," *Agricult. Water Manag.*, vol. 213, pp. 580–593, Mar. 2019.
- [30] Z. Fan, X. Zi-xuan, and W. Ming-hu, "State of health estimation for lithium battery using characteristic voltage intervals and genetic algorithm optimized back propagation neural network," *J. Energy Storage*, vol. 57, Jan. 2023, Art. no. 106277.
- [31] L. Wang, W. Ye, Y. Zhu, F. Yang, and Y. Zhou, "Optimal parameters selection of back propagation algorithm in the feedforward neural network," *Eng. Anal. Boundary Elements*, vol. 151, pp. 575–596, Jun. 2023.
- [32] Z.-L. Li, P. Leng, C. Zhou, K.-S. Chen, F.-C. Zhou, and G.-F. Shang, "Soil moisture retrieval from remote sensing measurements: Current knowledge and directions for the future," *Earth-Sci. Rev.*, vol. 218, Jul. 2021, Art. no. 103673.
- [33] J. Li, X. Wang, H. Jia, Y. Liu, Y. Zhao, C. Shi, F. Zhang, and K. Wang, "Assessing the soil moisture effects of planted vegetation on slope stability in shallow landslide-prone areas," *J. Soils Sediments*, vol. 21, no. 7, pp. 2551–2565, Jul. 2021.
- [34] A. S. Abowarda, L. Bai, C. Zhang, D. Long, X. Li, Q. Huang, and Z. Sun, "Generating surface soil moisture at 30 m spatial resolution using both data fusion and machine learning toward better water resources management at the field scale," *Remote Sens. Environ.*, vol. 255, Mar. 2021, Art. no. 112301.
- [35] B. W. Barrett, E. Dwyer, and P. Whelan, "Soil moisture retrieval from active spaceborne microwave observations: An evaluation of current techniques," *Remote Sens.*, vol. 1, no. 3, pp. 210–242, Jul. 2009.



YIFAN WANG received the Ph.D. degree in geodesy and survey engineering from China University of Mining and Technology, Xuzhou, China, in 2021. He is currently an Engineer with the Electric Power Research Institute, China Southern Power Grid Yunnan Power Grid Company Ltd. His current research interests include power grid operation and maintenance and disaster defense based on satellite technology.



YI MA received the bachelor's degree in high voltage technology and equipment from Shanghai Jiao Tong University, Shanghai, China, in 1992. He is currently a Professor Level Senior Engineer with the Electric Power Research Institute, China Southern Power Grid Yunnan Power Grid Company Ltd. His current research interests include grid disaster prevention and the intelligent operation and maintenance of power transmission.



FANGRONG ZHOU was born in Guizhou, China, in March 1982. He received the master's degree from the State Key Laboratory of Power Transmission Equipment and Security and New Technology, Chongqing University, in 2009. He is currently a Professor Level Senior Engineer with Yunnan Power Grid Company Ltd. His research interest includes power grid disaster prevention and reduction.



ZUGUI HUANG was born in Fangchenggang, Guangxi, China, in 1999. He received the B.S. degree in agricultural water resources engineering from Northwest A&F University, in 2022, where he is currently pursuing the master's degree in water resources engineering. His main research interest includes the efficient utilization of water resources based on optical remote sensing techniques.



YIFEI YAO received the Ph.D. degree in geodesy and survey engineering from China University of Mining and Technology, Xuzhou, China, in 2017. He is currently an Associate Professor with the College of Water Resources and Architectural Engineering, Northwest A&F University. His current research interests include upscaling and scale transitions, data fusion of multi-source remote sensing, and data assimilation.

...